LANGMUIR

pubs.acs.org/Langmuir Article

Deposition of Ultrathin MgB₂ Films from a Suspension Using Cosolvent Marangoni Flow

Thi Kieu Ngan Pham,* Edward Bruffey, III, Anh Tuan Nguyen, Ricardo A. Rivera-Maldonado, Ding-Yuan Kuo, Brandi Cossairt, Woochul Lee, Godwin Severa, and Joseph J. Brown



Cite This: Langmuir 2023, 39, 3853-3861



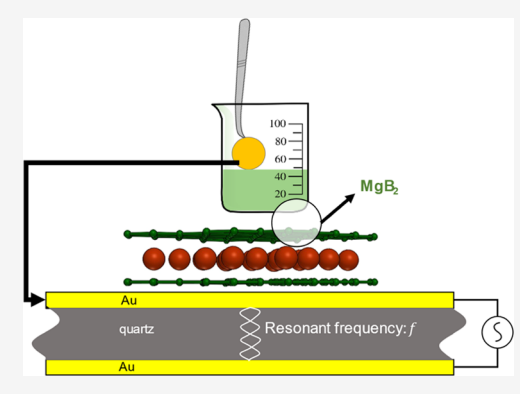
ACCESS |

III Metrics & More

Article Recommendations

s Supporting Information

ABSTRACT: Magnesium diboride (MgB₂) has demonstrated, theoretically and experimentally, promise as a candidate material for hydrogen storage and has thus attracted much contemporary research interest. To study hydrogen gas adsorption on MgB₂ thin films using a quartz crystal microbalance (QCM)—a workhorse apparatus for this specific experiment—MgB₂ must be deposited uniformly on the active surface of the QCM without damaging the quartz's performance. In work presented here, a wet-chemistry colloid synthesis and deposition process of a MgB₂ thin film on a gold (Au) surface was established to avoid the extreme conditions of conventional physical deposition methods. This process also counteracts the unwanted phenomena of drying droplets on a solid surface, particularly the coffee-ring effect. To verify the normal function of the QCM after MgB₂ deposition and its ability to obtain meaningful data, simple gas adsorption tests were conducted on the QCM, and the MgB₂ film on the QCM



was characterized with X-ray photoelectron spectroscopy (XPS) and atomic force microscopy (AFM) for elemental analysis and surface roughness, respectively. To obtain information about the thickness and the involvement of the coffee-ring effect, the same synthesis route was applied on a similar gold substrate—an evaporated Au film on glass. XPS characterization of the film and its precursor suspension shows the potential existence of both MgB_2 and its oxide forms. The film's thickness on evaporated Au was measured by scanning transmission electron microscopy (STEM) to be 3.9 nm. The resulting samples show mitigation of the coffeering effect through roughness measurements with AFM at two scan sizes of 50×50 and $1 \times 1 \ \mu m^2$.

■ INTRODUCTION

Hydrogen—the simplest element on Earth—has become a contemporary alternative for the energy industry to counteract the depletion of fossil fuels. As an efficient energy carrier, hydrogen gas has been extensively employed in multiple sectors, including refineries, aerospace technologies, semi-conductor manufacturing, fertilizer production, and many other chemical industries. A vision encompassing robust power generation from renewable energy rests upon the advancement of hydrogen storage research. Previous reviews of hydrogen storage methods highlighted chemical storage by metal hydrides as an alternative to physical storage approaches that require extreme pressure or temperature conditions (up to 800 bar for compression or down to 21.5 K for liquefaction) while also exhibiting favorable thermodynamic properties for hydrogen sorption and desorption.³

Magnesium borohydride ($Mg(BH_4)_2$) is a top candidate in the metal hydride family, thanks to its exceptionally high theoretical gravimetric (14.9 wt % H_2)⁴ and volumetric (147 g/L)⁵ hydrogen capacities and favorable enthalpy of hydrogen release ($\Delta H^0 = 38 \text{ kJ/mol } H_2$),⁶ which may allow for H_2 cycling between $Mg(BH_4)_2$ and MgB_2 at moderate pressures and temperatures. Early experimental work has shown varying

results. Severa et al. showed >11 wt % hydrogen reversibly stored in bulk MgB₂ at 400 °C, 950 bar.⁷ Liu et al. experimented on nanoplatelets of MgB₂, which were able to hydrogenate to Mg(BH₄)₂ at 280 °C and 700 bar. 8 Milder experimental conditions have been achieved via mechanical ball milling of the MgB₂ or through additive introduction. ⁹⁻¹¹ Our understanding of the reaction pathway between H₂ molecules and MgB2 is insufficient, with one highlighted publication from Ray et al. in 2017 elucidating the absorption mechanism involving hydrogen dissociation and diffusion into the MgB₂ lattice. 12 Also, in this work, the experiment was conducted on a volumetric Sievert apparatus, which is widely used for gas absorption experiments by measuring pressure change in a chamber 13 to plot hydrogen uptake. This method faces accumulative errors discussed elsewhere. 14 There is also a recent computational study elucidating hydrogenation at MgB₂

Received: October 27, 2022 Revised: March 2, 2023 Published: March 9, 2023





reactive edges, supporting the dissociation of H₂ molecules and later formation of molecular complexes. ¹⁵ Additionally, overcoming kinetic barriers to compensate for high working temperatures is an ongoing effort, not only for Mg(BH₄)₂ but also for many metal hydrides in general. ¹⁶ Slow reversibility kinetics of metal hydrides motivate research into nanoscale because a high surface-area-to-volume ratio potentially solves this problem. ^{17,18} This leads to a need for experimentation of hydrogen sorption on sorbent thin films. Magnesium diboride, whose chemical structure is comprised of two-dimensional nanosheets, is susceptible to both dry⁹ and wet¹⁹ exfoliation processes to increase its surface-area-to-volume ratio.

Meanwhile, the continued development of the quartz crystal microbalance (QCM) technology has offered more direct and advanced instrumentation for gas adsorption study, specifically on thin films, due to the excellent sensitivity and planar configuration of the QCM. The QCM is an electromechanical gravimetric sensor, which is able to detect ng/cm² of mass change on its surface by measuring the resonant frequency change of a quartz oscillator.²⁰ Because of its planar device configuration, rather than the convoluted surface configurations of many other adsorption sensing apparatus, the QCM can be adapted to enable gas adsorption experiments under external stimuli such as light or electric fields. ¹⁴ Computational work by Zhou et al. in 2010 predicted enhanced hydrogen storage on polarizable materials under applied electric fields.² Many further computational studies in recent years have predicted improved gas adsorption/sensitivity under applied electric fields. 21-25 A push toward experimental verification of this computational result requires novel experimental techniques, and the QCM completely prevails over other conventional volumetric/gravimetric apparatus in providing a feasible pathway to perform such experiments.

The H₂ gas adsorption experiment on a MgB₂ thin-film QCM drives this study to develop a synthesis route to deposit MgB₂ on the quartz crystal surface. As shown in Figure 1, the MgB₂ film is located on top of the gold (Au) electrode of the QCM. After depositing MgB2 on the Au electrode, the film must vibrate synchronously with the quartz and be uniformly distributed over the entire electrode surface²⁶ to obtain meaningful data.²⁷ Previous publications pertaining to the superconductivity of MgB2 used mostly hybrid physicalchemical vapor deposition (HPCVD) to deposit the MgB2 thin film on a substrate. This is a fast approach for industrial applications but inadequate for gas adsorption experiments on the QCM. The quartz used in the QCM traditionally works well under 300 °C and potentially exhibits phase transformation in the 500–600 $^{\circ}$ C range. HPCVD, whose working temperature is \sim 700–800 $^{\circ}$ C, $^{28-30}$ is thus inappropriate unless the film is mechanically transferred to the QCM after deposition on a different substrate.

This paper proposes a wet-chemistry synthesis and deposition route of MgB₂ thin films on the Au electrode of the QCM. Because MgB₂ is a layered material, we conduct delamination steps to obtain micro/nanostructures from bulk MgB₂ solid. These include heat treatment with anhydrous solvents, ball milling with and without solvents, and ultrasonication. There are various methods to deposit particles from the suspension phase onto a solid surface,³¹ of which all face a primary issue—the coffee-ring effect. The coffee-ring effect is a phenomenon in which particles inside a drop form a condensed ring at the perimeter as the drop dries. This means the nonuniform distribution of particles on the solid

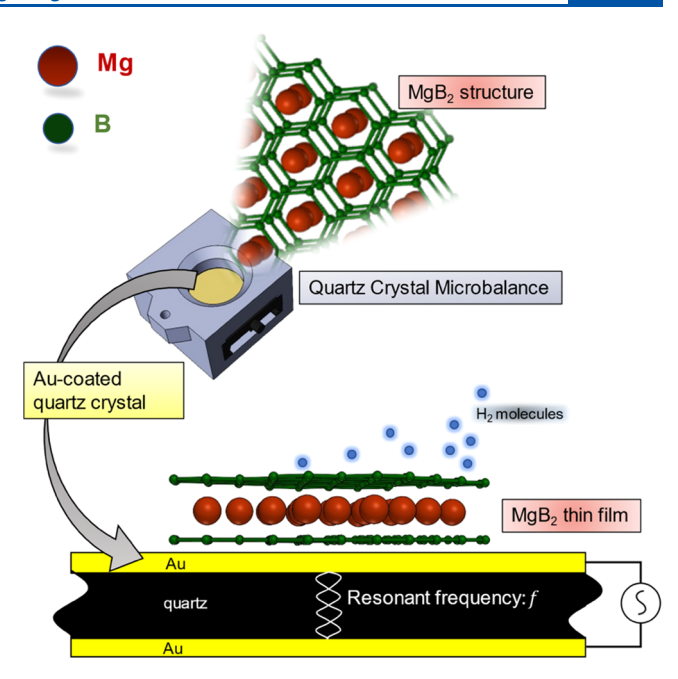


Figure 1. Display of gaseous H_2 adsorption on a MgB_2 thin film using a quartz crystal microbalance (QCM)—the three-layer configuration at the bottom. The QCM has an exposed gold surface, which is also its top electrode. Using the wet-chemistry synthesis route described in this paper, a MgB_2 thin film is deposited on this gold surface of the QCM. H_2 adsorption on MgB_2 is gravimetrically characterized by the quartz crystal microbalance, employing the piezoelectric effect.

surface, which is a nonoptimal result for controlled deposition of particle layers.³² This phenomenon was mathematically described by Deegan et al.³³ As the drop evaporates, its surface tends to lose liquid faster, but the drop cannot shrink due to surface pinning; this drives liquid flow from the center outward, thereby transporting suspended particles to the perimeter. Approaches to address the coffee-ring effect were extensively studied and summarized by Mampallil and Eral.³⁴ In the present paper, to counteract the unwanted coffee-ring effect, we used both thermal and solutal Marangoni flow using a cosolvent mixture to suspend MgB2 and then drying the sample on a hot plate (hot substrate). The use of a cosolvent mixture (two solvents A and B, in which boiling temperature: $T_{\text{boil, A}} > T_{\text{boil, B}}$ but surface tension: $\gamma_{\text{A}} < \gamma_{\text{B}}$) creates a surface tension gradient as the two solvents evaporate at different rates. This surface tension gradient creates an internal flow that brings particles from the periphery inward to the center. The difference in temperature between the substrate and the surrounding environment also creates a surface tension gradient, which suppresses the coffee-ring effect.³⁵ A graphical illustration of this Marangoni flow is presented in Figure 2. The high viscosity and high boiling point of the cosolvent ensure that the liquid does not evaporate too disruptively, thereby preserving internal laminar flow. After deposition, the resulting film was characterized with XPS, STEM, and AFM to identify the film's elemental identities, thickness, roughness, and particle distribution, respectively.

EXPERIMENTAL SECTION

An INFICON 14 mm diameter, 6 MHz, gold electrode AT-cut quartz crystal was purchased. Propylene glycol and dipropylene glycol were purchased from ThermoFisher. MgB_2 was purchased from Alfa Aesar. Anhydrous acetonitrile and anhydrous methanol were purchased from Sigma-Aldrich. Propylene glycol (PG) and dipropylene glycol (DPG)

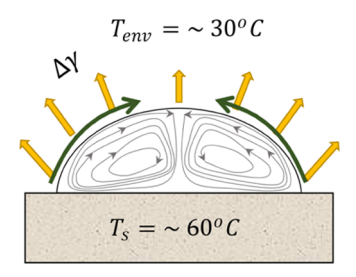


Figure 2. Illustration of the combined mass transport effect from both thermal and solutal Marangoni flow within a cosolvent droplet. The substrate remains at $\sim\!60$ °C and the environment is $\sim\!30$ °C. This temperature gradient creates thermal Marangoni flow. The lower-boiling-point solvent evaporates faster, and this leaves less quantity of this solvent, which has lower surface tension, at the center of the drop. This induced surface tension gradient creates a flow that brings more particles from the perimeter inward, known as solutal Marangoni flow.

were dried in a vacuum at 60 $^{\circ}$ C for 12 h and then stored with type 3A molecular sieves in an argon-filled glovebox. All synthetic processes of the MgB₂ suspension were performed under an argon atmosphere unless otherwise specified. In a typical process, \sim 1.2 g of MgB₂ and three 10 mm balls were added to each of the two Fritsch planetary ball mill vessels producing a 20:1 ball-to-powder ratio. Both the milling balls and pot were made of tungsten carbide. The ball mill was set to 700 rpm, having 5 min of forward run time and 5 min in reverse mode with a total forward run time of 2 h. Approximately, 0.2 g of the previously milled MgB₂ and 3 mL of acetonitrile were added to 10 mL minibatch Parr reactor vessels with a total of three vessels.

The total heat treatment time was 72 h, having the reactor set to 260 °C to reach an internal temperature reading of 250 °C. Upon completion of the heat treatment, MgB2 was transferred to a Schlenk flask and heated to 70 °C in vacuo for 2 h to remove the excess solvent. Then, 0.1 g of the prepared MgB₂ was then combined with 10 mL of a one-to-one PG/DPG mixture. This mixture was sonicated via tip sonication (Fisherbrand Ultrasonic Liquid Processor) with a 1/4" microtip at a 60% amplitude with 5 s on and 30 s off for a total on time of 1 h, and then passed through 0.2 μ m filters. Once complete, 1 mL aliquots were taken and diluted by differing factors, 1×, 5×, 10×, and 15x, with the target solvent. Aliquots from the dilutions were loaded into 1 mL centrifuge tubes and spun at 10 000 rpm for 30 min. The centrifugation step was conducted in an Eppendorf Centrifuge 5415 R in the open air. The top portion, which contains the target nanosheet MgB2, was carefully extracted in the open air and placed in a vial awaiting deposition. The 1:1 PG/DPG solution was contained in a beaker and heated up by a hot plate. As soon as the solution became stable at ~50 °C, the quartz crystal was immersed into the solution and then gradually removed from the solution at a rate of 0.01 mm/s. The quartz was then left in place to dry on a glass piece on top of the hot plate. This process was repeated twice. A graphical display of the experimental procedure is presented in Figure 3.

The MgB_2 -QCM quartz crystal was placed in an environmental control chamber 14 and exposed to two experimental conditions: (a) Argon flow (10 mL min $^{-1}$) at ambient temperature and (b) argon flow (10 mL min $^{-1}$) at $\sim\!68$ °C. The quartz's performance was evaluated through the recording of its frequency change through time. The quartz sample was also examined with XPS for elemental analysis and AFM for roughness. A similar synthesis route was applied to another gold film ($\sim\!100$ nm) on a glass substrate (evaporated Au) to evaluate the film thickness using STEM and the effect of the coffee-

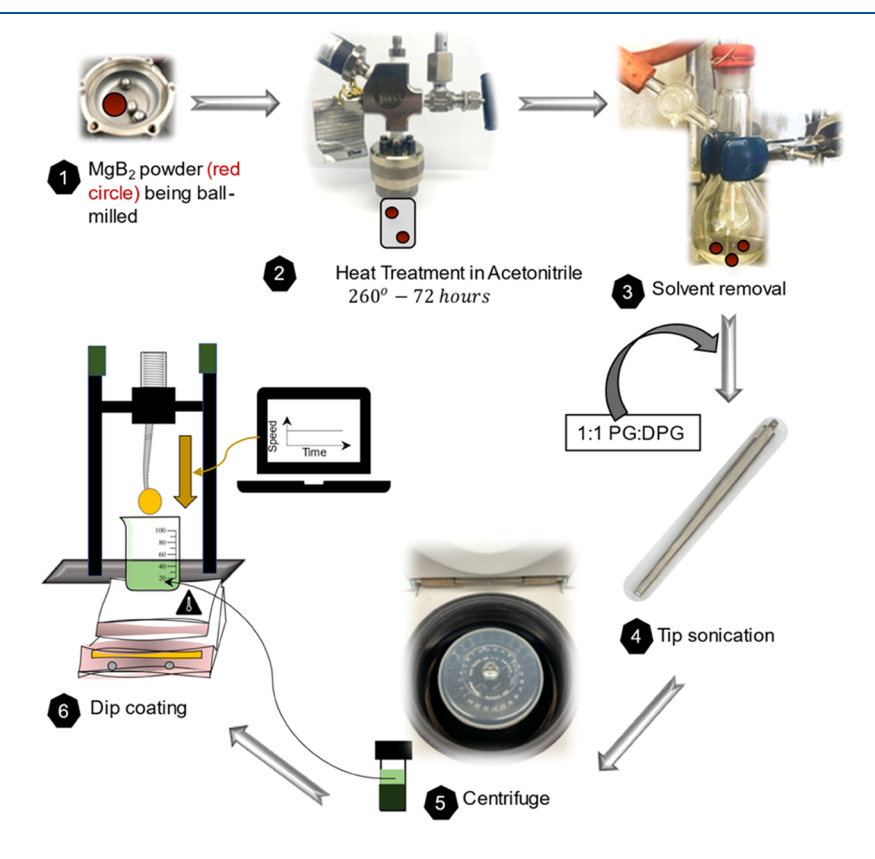


Figure 3. Schematic diagram of the synthetic procedure of the MgB_2 thin film on a QCM quartz crystal. Red circles represent MgB_2 particles. (1) The MgB_2 powder was ball-milled to reduce its size for better dilution in step 2. (2) MgB_2 particles were heat treated with acetonitrile in a minibatch Parr reactor. (3) The suspension was transferred to a Schlenk flask for solvent removal. (4) Prepared MgB_2 was dissolved in a 1:1 PG/DPG cosolvent, and the mixture was sonicated with a tip sonicator and filtered. (5) The aliquots were diluted and underwent centrifugation (the top portion in the suspension after centrifugation was the final MgB_2 in the PG/DPG solution). (6) The quartz crystal was immersed in this solution at a controlled rate of 0.01 mm/s at \sim 50 °C and left to dry on a glass surface.

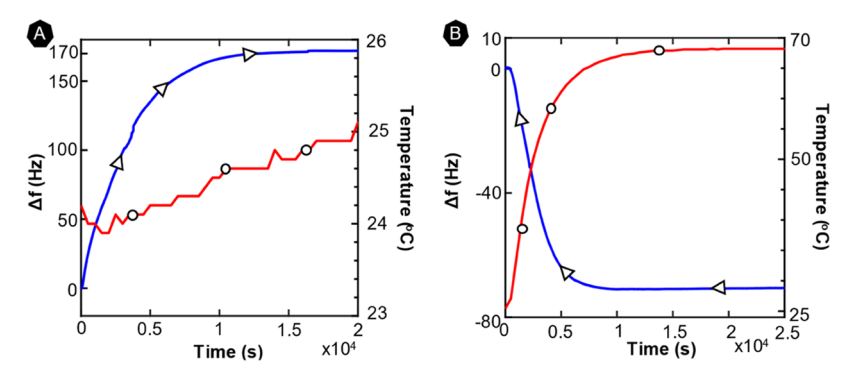


Figure 4. Frequency change of the MgB₂-deposited quartz crystal to temperature variation at two experimental conditions. (A) Argon flow at ambient temperature and (B) argon flow at ~68 °C. The blue triangular line represents the frequency change Δf and the red circular line represents the temperature T.

ring effect via roughness measurement on AFM. Identification of elements in the film was conducted in the XPS Kratos AXIS Ultra DLD using a monochromatized Al K α X-ray and a low-energy electron flood gun for charge neutralization. Each XPS spectrum was calibrated by assigning the Au 4f_{7/2} peak to 84 eV or the C 1s peak to 284.8 eV if Au was not detected in the sample. X-ray spot size for these acquisitions was on the order of 700 \times 300 μ m². The pressure in the analytical chamber during spectral acquisition was less than 5 × 10⁻⁹ Torr. The pass energy for survey spectra (composition) was 80 eV. The pass energy for the high-resolution spectra was 20 eV. The take-off angle (the angle between the sample normal and the input axis of the energy analyzer) was 0° (0° take-off angle, ~100 Å sampling depth). Kratos Vision2 software was used to determine peak areas and to calculate the elemental compositions from peak areas. The film thickness was measured by STEM at 200 kV on an FEI Tecnai G2 F20 Supertwin TEM with STEM capabilities using a highangle annular dark-field imaging (HAADF) detector. AFM characterization was performed using a Park NX10 operating in noncontact mode to obtain the topography and surface roughness of the film with a scan size of 50 \times 50 and 1 \times 1 μ m²; an NCHR probe (spring constant = 42 N/m) was used to perform roughness measurements.

RESULTS AND DISCUSSION

As shown in Figure 4, the quartz's frequency varies with temperature. The frequency fluctuation with temperature is

Table 1. XPS Results of the MgB_2 Film Deposited on the QCM Quartz Crystal

element	peak	B.E. (eV)	atomic percentage (%)
Mg	1s	1304	2.81
Na	1s	1072	0.83
O	1s	532	17.42
N	1s	399	9.33
С	1s	285	61.23
Cl	2p	201	4.47
Au	4f	84	3.9

expected because the quartz crystal resonates differently at different temperatures, and its performance fits with a previous study on the same kind of quartz crystal and the QCM manufacturer. However, experiments to identify MgB2-deposited quartz crystal's optimal working temperature are not within this paper's scope. The MgB2-deposited quartz crystal has a recorded frequency of $\sim 5\,979\,227\,$ Hz, decreased $\sim 130\,$ Hz from that of the unloaded one. Theoretically, the deposited layer creates a mass loading on the quartz, resulting in a new resonant frequency, which can be calculated via the Z-match theory (eq 1). There is no defined density for the MgB2

Table 2. XPS Results of MgB₂ Drop Cast on an Arbitrary Glass Surface

element	peak	B.E. (eV)	atomic percentage (%)
Mg	1s	1304	1.8
Na	1s	1072	3.37
O	1s	532	24.26
N	1s	399	12.94
С	1s	285	54.29
Cl	2p	201	0.58
S	2p	168	0.5
В	1s	192.2	2.26

film, but within an estimated range of 1-2.5 g cm⁻³, the approximated thickness of deposited MgB₂ was in the range of 2-7 nm, which is consistent with our other characterization results

$$TK = \left(\frac{N_{q} \times \rho_{q}}{\pi \times R_{z} \times f \times \rho_{f}}\right) \arctan \left[R_{z}\right]$$

$$\times \tan \left[\pi \times \left(\frac{f_{q} - f}{f}\right)\right]$$
(1)

where TK = thickness of the MgB₂ film (cm), $N_{\rm q}$ = 1.668 × 10^5 Hz × cm is the frequency constant for the AT-cut quartz crystal, $\rho_{\rm q}$ = 2.648 g cm⁻³ is the quartz' density, $R_{\rm z}$ is the Z-factor of MgB₂, $\rho_{\rm f}$ is MgB₂'s density, and $f_{\rm q}$ (Hz) = 5 979 361 and f (Hz) = 5 979 227 are frequencies of quartz without and with the MgB₂ layer, respectively.

The XPS result of the MgB₂ film deposited on the QCM quartz crystal (Table 1) shows the Mg element at a 2.81% atomic concentration. The survey spectrum is presented in Chart S1, with a distinct peak of Mg 2p at 50 eV but none for B 1s in the known region for B compounds. 36 The presence of Mg and B on the samples was also verified with EDS (energydispersive spectroscopy) on TEM but was not successful. Results are reported in Chart S2. It was challenging to do elemental analysis directly on the film because of the film's thinness and EDS' limitation in detecting low-atomic number elements like boron. A thicker film was created by randomly drop-casting 50 µL of the MgB₂ suspension on a glass substrate, with the resulting film later characterized with XPS. The result, as shown in Table 2, exhibited distinct peaks of Mg and B. The high-resolution scans of Mg 2p and B1 s on this film are presented in Figure 5. There are Mg 2p at 50 eV,

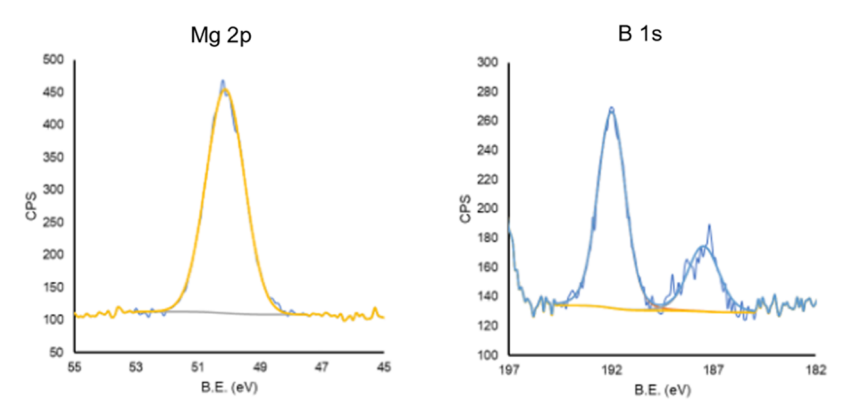


Figure 5. High-resolution scans of Mg 2p and B 1s from the drop-casting sample by XPS to determine the presence of MgB₂ and its oxides.

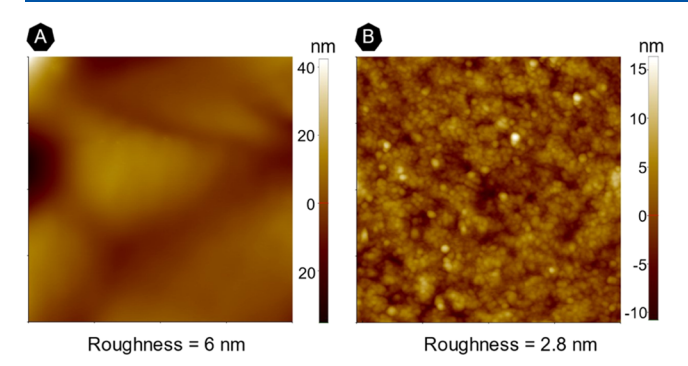


Figure 6. Topography images of the QCM quartz crystal obtained from AFM characterization. (A) QCM quartz crystal before MgB₂ deposition (roughness = 6 nm). (B) QCM quartz crystal after MgB₂ deposition (roughness = 2.8 nm). The scan size is $1 \times 1 \ \mu m^2$.

which can be both MgB2 and MgO, and B 1s at 188 eV for MgB₂ and 192 eV for B₂O₃.8 In conclusion, we were unable to confirm the presence of MgB₂ in the film by conducting XPS directly with the thin MgB2 film on the QCM quartz crystal. However, XPS results from the precursor suspension confirm the presence of MgB2 in a thick film with the potential presence of MgO and B₂O₃. This compositional information should reflect that of the thin MgB2 film on the QCM quartz crystal as well. The observed high content of C in XPS data is attributed to solvent residuals. Simultaneously, the low B/Mg ratio (1:0.8) was witnessed earlier by Liu et al., in which the MgB₂ nanoplatelets experienced composition change and strain, surface termination of the B sheets, and B-B disorder.8 Regarding other elements in both tables, the presence of Au (Table 1) is expected because the film was deposited on Au. The 9.3% signal from N can be attributed to residual contamination from acetonitrile during the synthesis process. Na and Cl are likely from salt NaCl from human's body sweat.

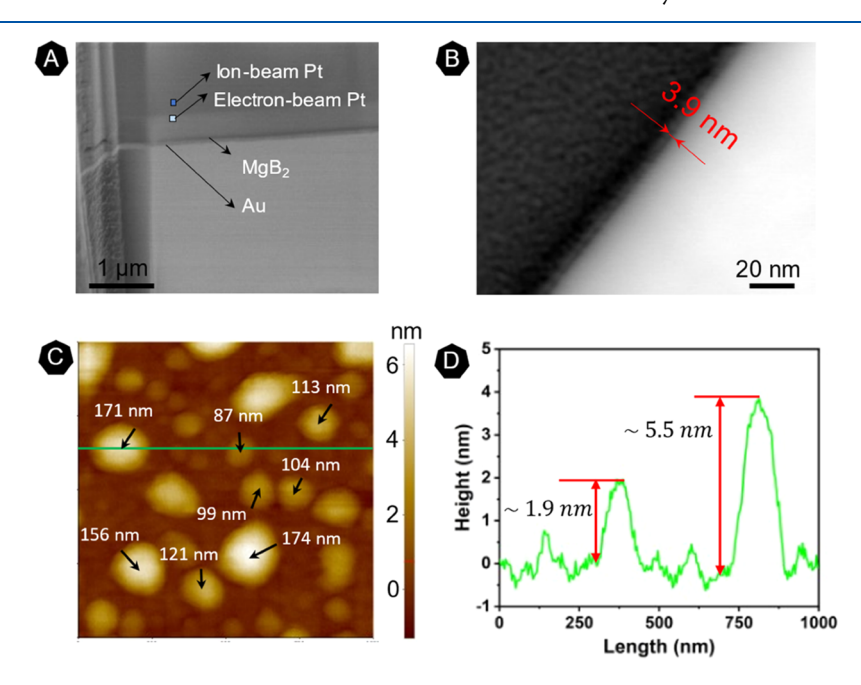


Figure 7. Film thickness verification. (A) SEM image of the FIB-cut MgB_2 sample on evaporated Au, protected by Pt layers. This sample was prepared for STEM, so layers of Pt were developed on top of the MgB_2 layer to bind to the tip transferring the sample piece to the TEM grid without damaging MgB_2 . (B) STEM image indicating 3.9 nm thickness. (C) Topography of the MgB_2 sample on the silicon wafer, showing multiple separate particles with a height ranging around 1.7–6.7 nm. In this measurement, we used contact mode with a CONTSCR probe (spring constant = 0.2 N/m) under the constant force of 15 nN. The average particle height of 3.84 nm is in good agreement with the film thickness of 3.9 nm measured by STEM. The scan size is $1 \times 1 \ \mu m^2$. (D) Extraction of the horizontal line (green) in (C) to elucidate the height of the particles.

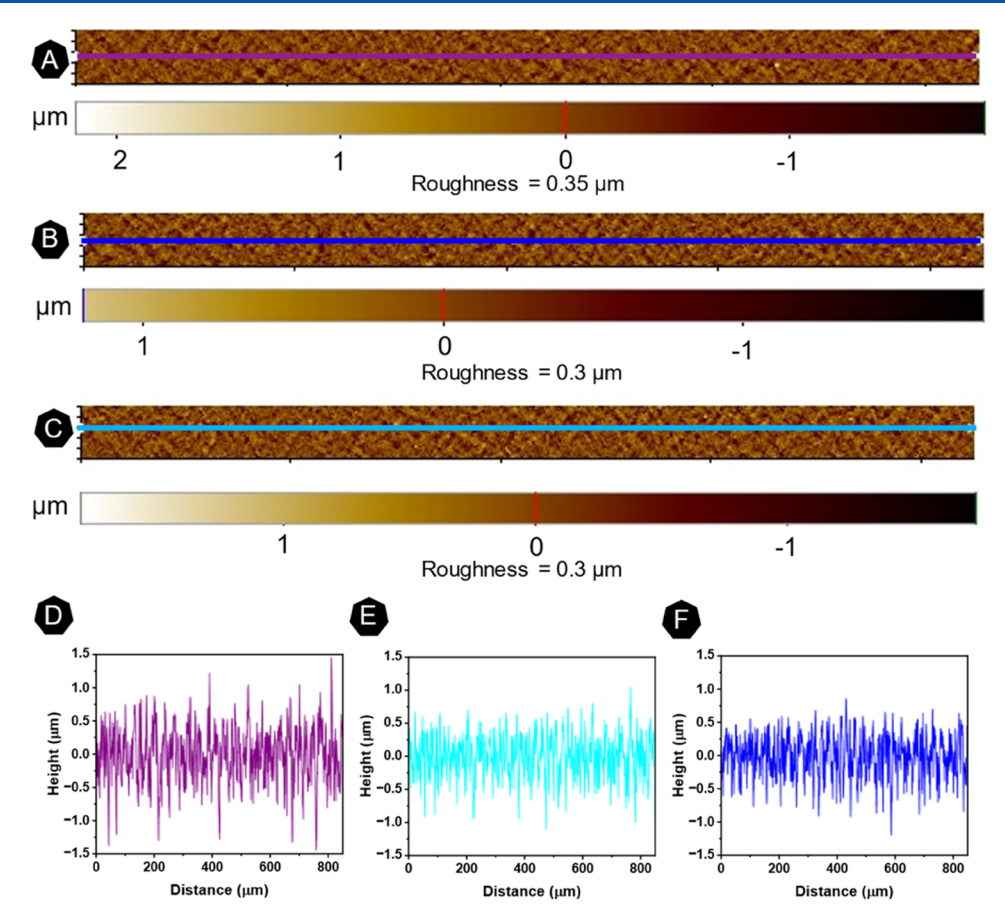


Figure 8. AFM characterization of MgB₂ on the QCM Au to evaluate the Marangoni effect. (A–C) Topographies of the QCM Au (the size of 850 μ m × 50 μ m) at the periphery (A), at ~3 mm from the center (B), and at the center (C). In AFM characterization, a measurement size of 50 μ m × 50 μ m was captured; 850- μ m-long topography was achieved through 17 continuous images. Line extraction topography evaluated was to elucidate the height variation of the QCM Au sample from the topographies at the periphery (D), at ~3 mm from the center (E), and at the center (F). Roughnesses at these three positions are 0.35, 0.3, and 0.3 μ m, respectively.

The AFM image in Figure 6A shows the original QCM quartz crystal having a valley-like topography with a surface roughness of 6 nm in the 1 μ m \times 1 μ m scanning area. After deposition, the MgB₂ particles spread over the surface, reducing the surface roughness from 6 nm to 2.8 nm (Figure 6B). Because the surface roughness of the original QCM quartz crystal is significantly large compared to the thickness of the MgB₂ film, it is very challenging to measure the MgB₂ film's thickness on the QCM quartz crystal directly by AFM.

To measure the thickness of the MgB₂ layer on Au, we repeated the synthesis route on the evaporated Au. We note that the evaporated Au surface was very flat, as its initial surface roughness was 0.29 nm (see Figure S1). STEM was conducted at 200 kV to provide ample resolution to allocate the MgB₂ layer from a FIB (focus ion beam)-cut sample, as shown in Figure 7A. Figure 7B shows an average value of thickness of 3.9 nm. The statistical analysis to obtain the average height of the particles on evaporated Au is presented in Table S1. This is in good accordance with independently measured particle heights by AFM (Figure 7C,D), in which the same experimental procedure was applied on a silicon wafer—an another flat substrate (surface roughness of 0.11 nm, see Figure S2).

An important element for obtaining consistent data in future gas adsorption on the MgB₂-QCM quartz crystal is to have a uniformly deposited film on its electrode (Au) surface. As discussed in the introduction, we use Marangoni flow to counteract the unwanted coffee-ring effect, and this effect was

first evaluated by conducting a range of AFM scanning of 850 μ m \times 50 μ m using a stitch function. A total of 17 continuous scans at each of the three positions, at the periphery (Figure 8A), at \sim 3 mm from the periphery (Figure 8B), and at the center (Figure 8C) of the quartz crystal, were conducted. An exemplary individual topography at this wide scan size is shown in Figure S3. There was only a 16% difference between roughness at the center and at the periphery. Based on the line extraction topographies, as shown in Figure 8D–F, we observed similar topography features among three positions, and there was no irregular peak (indication of the coffee-ring effect) seen at any position within every 850 μ m range.

To further understand the coffee-ring effect at the nanoscale, we measured film topographies at a scan size of $1 \times 1~\mu\text{m}^2$ at three different positions: the center and two peripheral areas, as shown in Figure 9. We note that at this small scan size, the roughness was evaluated on evaporated Au instead of the QCM Au because of the significant difference in roughness between the QCM Au and MgB₂ film, as mentioned above. The three positions have different roughnesses (two peripheral areas: 1.86 nm, 2 nm; center: 1.55 nm), with a rougher surface at the periphery than in the center. The induced Marangoni flow significantly reduced the coffee-ring effect with a 16% roughness difference at a scan size of $50 \times 50~\mu\text{m}^2$ and ~20% for a scan size of $1 \times 1~\mu\text{m}^2$ for different measuring positions on the samples. Under an optical microscope, the coffee-ring

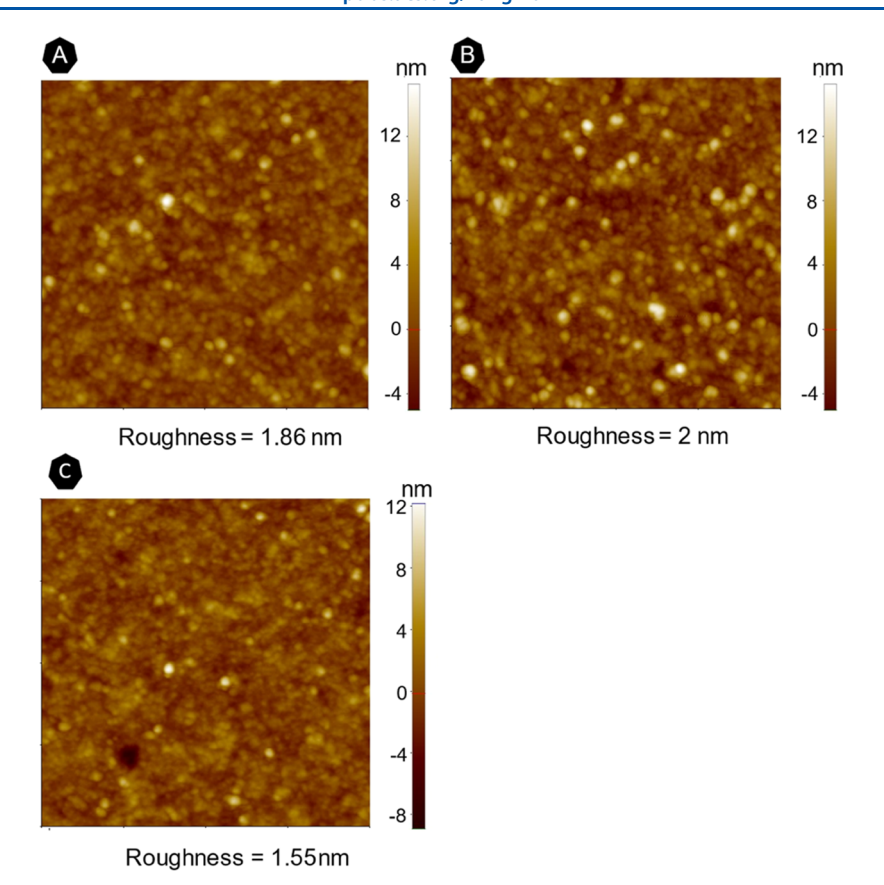


Figure 9. Topography images of MgB₂ on the evaporated Au substrate at three positions. The AFM measurement was done at (A, B) peripheral positions and (C) center position of the substrate. The coffee-ring effect was not fully eliminated, indicated by the difference in roughness at three positions: (A) roughness = 1.86 nm, (B) roughness = 2 nm, and (C) roughness = 1.55 nm. The scan size is $1 \times 1 \mu m^2$.

rim was very visible without the contribution from Marangoni flow (see Figure S4).

CONCLUSIONS

A wet-chemistry cosolvent approach to engineer the Marangoni effect allowed the deposition of a uniform MgB₂ film onto the Au electrode of a QCM quartz crystal. Such lowcost, controlled deposition is needed to enable both physical science and manufacturing with novel energy storage materials such as MgB₂. After colloid deposition via cosolvent evaporation, the MgB2-deposited quartz crystal functions normally, with a reasonable frequency shift from its original resonant frequency. AFM data showed the effectiveness of the cosolvent Marangoni engineering to mitigate the coffee-ring effect. This is a crucial step to use the QCM, a highly sensitive gravimetric detector, to study minute changes of H2 absorption in MgB2, and we anticipate that similar approaches may be taken for the deposition of particle thin films from suspensions. XPS results directly from the film were not sufficient to prove the presence of MgB₂, but that of the precursor solution shows the peak of Mg and B, showing both MgB2 and oxides (MgO and B₂O₃). The average film thickness of deposited MgB₂ on evaporated Au was confirmed to be 3.9 nm by STEM. This thin layer ensures that MgB₂ vibrates synchronously with the quartz. This also means that the proposed wet-chemistry synthesis can provide a few nanometers thick film of a layered material, not limiting the options to physical methods. This process generally promotes the application of the QCM in the study of gas adsorption on the thin film, especially those of a few monolayers, as in this paper (\sim 3.9 nm).

ASSOCIATED CONTENT

Supporting Information

The Supporting Information is available free of charge at https://pubs.acs.org/doi/10.1021/acs.langmuir.2c02933.

EDS characterization of MgB_2 –QCM Au, table of MgB_2 film thickness measurements at 27 positions, and AFM 2D image of the evaporated Au layer on a glass substrate (PDF)

AUTHOR INFORMATION

Corresponding Author

Thi Kieu Ngan Pham – Department of Mechanical Engineering, University of Hawai'i at Mānoa, Honolulu, Hawai'i 96822, United States; Email: tknp@hawaii.edu

Authors

Edward Bruffey, III — Department of Mechanical Engineering, University of Hawai'i at Mānoa, Honolulu, Hawai'i 96822, United States; Hawaii Natural Energy Institute, University of Hawai'i at Mānoa, Honolulu, Hawai'i 96822, United States

Anh Tuan Nguyen — Department of Mechanical Engineering, University of Hawai'i at Manoa, Honolulu, Hawai'i 96822, United States; orcid.org/0000-0002-1441-9705

Ricardo A. Rivera-Maldonado — Department of Chemistry, University of Washington, Seattle, Washington 98195, United States

Ding-Yuan Kuo – Department of Chemistry, University of Washington, Seattle, Washington 98195, United States

- Brandi Cossairt Department of Chemistry, University of Washington, Seattle, Washington 98195, United States
- Woochul Lee Department of Mechanical Engineering, University of Hawai'i at Manoa, Honolulu, Hawai'i 96822, United States; ⊚ orcid.org/0000-0002-0911-961X
- Godwin Severa Hawaii Natural Energy Institute, University of Hawai'i at Mānoa, Honolulu, Hawai'i 96822, United States; Occid.org/0000-0002-1695-9123
- Joseph J. Brown Department of Mechanical Engineering, University of Hawai'i at Manoa, Honolulu, Hawai'i 96822, United States

Complete contact information is available at: https://pubs.acs.org/10.1021/acs.langmuir.2c02933

Author Contributions

This manuscript was written through the contributions of all authors. All authors have given approval to the final version of the manuscript.

Funding

Department of Energy (Grant Number DE-SC0020213): "Fostering a Guided Multiscale Model for the Development of Advanced MgB₂ Hydrogen Storage Materials". NSF (Grant Number DMR-2121848): University of Hawaii—University of Washington "PREM: Materials Research and Education Consortium (MRE-C)". NSF Grant Number DMR-1719797.

Notes

The authors declare no competing financial interest.

ACKNOWLEDGMENTS

The authors greatly appreciate useful communications with Dr. Craig Jensen from the Chemistry Department, University of Hawai'i at Manoa, Hawai'i, USA.

ABBREVIATIONS

QCM, quartz crystal microbalance; XPS, X-ray photoelectron spectroscopy; STEM, transmission electron microscopy; AFM, atomic force microscopy; EDS, energy-dispersive detector

REFERENCES

- (1) Pham, T. K. N.; Brown, J. J. Hydrogen Sensors Using 2-Dimensional Materials: A Review. *ChemistrySelect* **2020**, *5*, 7277–7297.
- (2) Zhou, J.; Wang, Q.; Sun, Q.; Jena, P.; Chen, X. S. Electric Field Enhanced Hydrogen Storage on Polarizable Materials Substrates. *Proc. Natl. Acad. Sci. U.S.A.* **2010**, *107*, 2801–2806.
- (3) Niaz, S.; Manzoor, T.; Pandith, A. H. Hydrogen Storage: Materials, Methods and Perspectives. *Renewable Sustainable Energy Rev.* **2015**, *50*, 457–469.
- (4) Nakamori, Y.; Orimo, S. Borohydrides as Hydrogen Storage Materials. In *Solid-State Hydrogen Storage*; Elsevier, 2008; pp 420–449.
- (5) Filinchuk, Y.; Richter, B.; Jensen, T. R.; Dmitriev, V.; Chernyshov, D.; Hagemann, H. Porous and Dense Magnesium Borohydride Frameworks: Synthesis, Stability, and Reversible Absorption of Guest Species. *Angew. Chem., Int. Ed.* **2011**, 50, 11162–11166.
- (6) van Setten, M. J.; de Wijs, G. A.; Fichtner, M.; Brocks, G. A Density Functional Study of α -Mg(BH₄)₂. *Chem. Mater.* **2008**, 20, 4952–4956.
- (7) Severa, G.; Rönnebro, E.; Jensen, C. M. Direct Hydrogenation of Magnesium Boride to Magnesium Borohydride: Demonstration of >11 Weight Percent Reversible Hydrogenstorage. *Chem. Commun.* **2010**, *46*, 421–423.

- (8) Liu, Y.-S.; Ray, K. G.; Jørgensen, M.; Mattox, T. M.; Cowgill, D. F.; Eshelman, H. V.; Sawvel, A. M.; Snider, J. L.; York, W.; Wijeratne, P.; et al. Nanoscale Mg—B via Surfactant Ball Milling of MgB2: Morphology, Composition, and Improved Hydrogen Storage Properties. J. Phys. Chem. C 2020, 124, 21761—21771.
- (9) Sugai, C.; Kim, S.; Severa, G.; White, J. L.; Leick, N.; Martinez, M. B.; Gennett, T.; Stavila, V.; Jensen, C. Kinetic Enhancement of Direct Hydrogenation of MgB₂ to Mg(BH₄)₂ upon Mechanical Milling with THF, MgH₂, and/or Mg. *ChemPhysChem* **2019**, 20, 1301–1304.
- (10) Newhouse, R. J.; Stavila, V.; Hwang, S.-J.; Klebanoff, L. E.; Zhang, J. Z. Reversibility and Improved Hydrogen Release of Magnesium Borohydride. *J. Phys. Chem. C* **2010**, *114*, 5224–5232.
- (11) Snider, J. L.; Mattox, T. M.; Liu, Y.-S.; Wan, L. F.; Wijeratne, P.; Allendorf, M. D.; Stavila, V.; Wood, B. C.; Klebanoff, L. E. The Influence of LiH and TiH₂ on Hydrogen Storage in MgB₂ II. XPS Study of Surface and near-Surface Phenomena. *Int. J. Hydrogen Energy* **2022**, *47*, 403–419.
- (12) Ray, K. G.; Klebanoff, L. E.; Lee, J. R. I.; Stavila, V.; Heo, T. W.; Shea, P.; Baker, A. A.; Kang, S.; Bagge-Hansen, M.; Liu, Y.-S.; White, J. L.; Wood, B. C. Elucidating the Mechanism of MgB₂ Initial Hydrogenation via a Combined Experimental—Theoretical Study. *Phys. Chem. Chem. Phys.* **2017**, *19*, 22646—22658.
- (13) Voskuilen, T.; Zheng, Y.; Pourpoint, T. Development of a Sievert Apparatus for Characterization of High Pressure Hydrogen Sorption Materials. *Int. J. Hydrogen Energy* **2010**, *35*, 10387–10395.
- (14) Pham, T. K. N.; Garcia, G. A.; Brown, J. J. Measurement of Isosteric Heat of Gas Adsorption and Brunauer–Emmett–Teller (BET) Surface Area Using a Quartz Crystal Microbalance. *Rev. Sci. Instrum.* 2022, 93, No. 064105.
- (15) Ray, K. G.; Klebanoff, L. E.; Stavila, V.; Kang, S.; Wan, L. F.; Li, S.; Heo, T. W.; Allendorf, M. D.; Lee, J. R. I.; Baker, A. A.; Wood, B. C. Understanding Hydrogenation Chemistry at MgB₂ Reactive Edges from *Ab Initio* Molecular Dynamics. *ACS Appl. Mater. Interfaces* **2022**, 14, 20430–20442.
- (16) Klebanoff, L. E.; Keller, J. O. 5 Years of Hydrogen Storage Research in the U.S. DOE Metal Hydride Center of Excellence (MHCoE). *Int. J. Hydrogen Energy* **2013**, 38, 4533–4576.
- (17) Wood, B. C.; Heo, T. W.; Kang, S.; Wan, L. F.; Li, S. Beyond Idealized Models of Nanoscale Metal Hydrides for Hydrogen Storage. *Ind. Eng. Chem. Res.* **2020**, *59*, 5786–5796.
- (18) Gunda, H.; Ray, K. G.; Klebanoff, L. E.; Dun, C.; Marple, M. A. T.; Li, S.; Sharma, P.; Friddle, R. W.; Sugar, J. D.; Snider, J. L.; Horton, R. D.; Davis, B. C.; Chames, J. M.; Liu, Y.-S.; Guo, J.; Mason, H. E.; Urban, J. J.; Wood, B. C.; Allendorf, M. D.; Jasuja, K.; Stavila, V. Hydrogen Storage in Partially Exfoliated Magnesium Diboride Multilayers. *Small* **2023**, *19*, No. 2205487.
- (19) Gilliam, M. S.; Yousaf, A.; Guo, Y.; Li, D. O.; Momenah, A.; Wang, Q. H.; Green, A. A. Evaluating the Exfoliation Efficiency of Quasi-2D Metal Diboride Nanosheets Using Hansen Solubility Parameters. *Langmuir* **2021**, *37*, 1194–1205.
- (20) Dultsev, F. N.; Kolosovsky, E. A. QCM Operating in Threshold Mode as a Gas Sensor. *Langmuir* **2009**, *25*, 12195–12200.
- (21) Razmkhah, M.; Mosavian, M. T. H.; Moosavi, F.; Ahmadpour, A. CO2 Gas Adsorption into Graphene Oxide Framework: Effect of Electric and Magnetic Field. *Appl. Surf. Sci.* **2018**, *456*, 318–327.
- (22) Ai, W.; Kou, L.; Hu, X.; Wang, Y.; Krasheninnikov, A. V.; Sun, L.; Shen, X. Enhanced Sensitivity of MoSe ₂ Monolayer for Gas Adsorption Induced by Electric Field. *J. Phys.: Condens. Matter* **2019**, *31*, No. 445301.
- (23) Liang, X.-Y.; Ding, N.; Ng, S.-P.; Wu, C.-M. L. Adsorption of Gas Molecules on Ga-Doped Graphene and Effect of Applied Electric Field: A DFT Study. *Appl. Surf. Sci.* **2017**, *411*, 11–17.
- (24) Yue, Q.; Shao, Z.; Chang, S.; Li, J. Adsorption of Gas Molecules on Monolayer MoS2 and Effect of Applied Electric Field. *Nanoscale Res. Lett.* **2013**, *8*, 425.
- (25) Yu, J.; He, C.; Huo, J.; Zhao, C.; Yu, L. Adsorption and Electric Field Assisted Activation of Ammonia-Borane over BC₃ Sheet: A Computational Study. *Int. J. Hydrogen Energy* **2022**, 47, 7738–7750.

- (26) Zhang, P.; Hu, W.; Wu, M.; Gong, L.; Tang, A.; Xiang, L.; Zhu, B.; Zhu, L.; Zeng, H. Cost-Effective Strategy for Surface Modification via Complexation of Disassembled Polydopamine with Fe(III) Ions. *Langmuir* **2019**, *35*, 4101–4109.
- (27) Lu, C.; Czanderna, A. W. Applications of Piezoelectric Quartz Crystal Microbalances; Elsevier, 2012; Vol. 7, pp 197–217.
- (28) Seong, W. K.; Huh, J. Y.; Kang, W. N.; Kim, J.-W.; Kwon, Y.-S.; Yang, N.-K.; Park, J.-G. Growth of Epitaxial MgB₂ Thick Films with Columnar Structures by Using HPCVD. Chem. Vap. Deposition 2007, 13, 680–683.
- (29) Guo, Z.; Cai, X.; Yang, C.; Niu, R.; Liao, X.; Chen, Y.; Zhang, Y.; Luo, W.; Huang, Z.; Feng, Q.; Gan, Z. The Preparation of Cylindrical MgB₂ Films on Stainless Steel by HPCVD for Magnetic Shielding. *Physica C* **2018**, *551*, 28–32.
- (30) Lee, N.; Withanage, W. K.; Tan, T.; Wolak, M. A.; Nassiri, A.; Xi, X. Hybrid Physical Chemical Vapor Deposition of Magnesium Diboride inside 3.9 GHz Mock Cavities. *IEEE Trans. Appl. Supercond.* **2016**, 27, 1–4.
- (31) Sharma, R.; Strano, M. S. Centerline Placement and Alignment of Anisotropic Nanotubes in High Aspect Ratio Cylindrical Droplets of Nanometer Diameter. *Adv. Mater.* **2009**, *21*, 60–65.
- (32) Katre, P.; Balusamy, S.; Banerjee, S.; Sahu, K. C. An Experimental Investigation of Evaporation of Ethanol—Water Droplets Laden with Alumina Nanoparticles on a Critically Inclined Heated Substrate. *Langmuir* **2022**, *38*, 4722–4735.
- (33) Deegan, R. D.; Bakajin, O.; Dupont, T. F.; Huber, G.; Nagel, S. R.; Witten, T. A. Capillary Flow as the Cause of Ring Stains from Dried Liquid Drops. *Nature* **1997**, *389*, 827–829.
- (34) Mampallil, D.; Eral, H. B. A Review on Suppression and Utilization of the Coffee-Ring Effect. *Adv. Colloid Interface Sci.* **2018**, 252, 38–54.
- (35) Lee, S. Y.; Kim, H.; Kim, S.-H.; Stone, H. A. Uniform Coating of Self-Assembled Non-Iridescent Colloidal Nanostructures Using Marangoni Effects and Polymers. *Phys. Rev. Appl.* **2018**, *10*, No. 054003.
- (36) Liu, Y.-S.; Klebanoff, L. E.; Wijeratne, P.; Cowgill, D. F.; Stavila, V.; Heo, T. W.; Kang, S.; Baker, A. A.; Lee, J. R. I.; Mattox, T. M.; Ray, K. G.; Sugar, J. D.; Wood, B. C. Investigating Possible Kinetic Limitations to MgB₂ Hydrogenation. *Int. J. Hydrogen Energy* **2019**, 44, 31239–31256.

☐ Recommended by ACS

Preparation and Characterization of a Coordination Polymer Based on Iron (III)-Cyamelurate as a Superior Catalyst for Heterogeneous Fenton-Like Processes

Wanessa Lima de Oliveira, João Paulo de Mesquita, et al.

MARCH 29, 2023

LANGMUIR

READ 🗹

Kinetic Monte Carlo Study on the Role of Heterogeneity in the Dissolution Kinetics of Glasses

Luis Ruiz Pestana, Prannoy Suraneni, et al.

APRIL 18, 2023

THE JOURNAL OF PHYSICAL CHEMISTRY C

READ 🗹

Flexible Graphite Nanoflake/Polydimethylsiloxane Nanocomposites with Promising Solar–Thermal Conversion Performance

Suman Chhetri, Woochul Lee, et al.

FEBRUARY 03, 2023

ACS APPLIED ENERGY MATERIALS

READ **C**

Al/CuF₂ Composite Materials with Ignition Characteristics and Pressure Output Ability for Nanothermites

Jie Ji, Xiaode Guo, et al.

FEBRUARY 08, 2023

ACS APPLIED NANO MATERIALS

READ 🗹

Get More Suggestions >